In vitro assessment of real-time phase contrast MRI accuracy

Pan LIU (liupanronald@hotmail.com)
CHU Amiens-Picardie: Centre Hospitalier Universitaire Amiens-Picardie https://orcid.org/0000-0003-0559-6432
Sidy FALL
University of Picardy Jules Verne: Universite de Picardie Jules Verne
Maureen AHIATSI
University of Picardy Jules Verne: Universite de Picardie Jules Verne
Olivier BALEDENT
CHU Amiens-Picardie: Centre Hospitalier Universitaire Amiens-Picardie

Research article

Keywords: phase-contrast, echo-planar imaging, cine MRI, pulsatile flow, imaging phantom

Posted Date: February 18th, 2022

DOI: https://doi.org/10.21203/rs.3.rs-1334567/v1

In vitro assessment of real-time phase contrast MRI accuracy

Pan Liu[1,2], Sidy Fall[3], Maureen Ahiatsi [1], Olivier Baledent[1,2,3]

[1] CHIMERE UR 7516, Jules Verne University of Picardy, Amiens, France.

[2] Medical Image Processing Department, Amiens Picardy University Hospital, Amiens, France

[3] MRI Department, Jules Verne University of Picardy, Amiens, France

Sidy Fall: sidy.fall@u-picardie.fr

Maureen Ahiatsi: maureenahiatsi@hotmail.com

Olivier Baledent: olivier.baledent@chu-amiens.fr

Corresponding Author

Family Name: Liu

Given Name: Pan

ORCID: https://orcid.org/0000-0003-0559-6432

E-mail: liupanronald@hotmail.com

Phone: +33-770-335-351

Total number of words: 4691

Number of words of the abstract:313

Number of figures: 9 + 1 graphical abstract

Number of tables: 3

Abstract

Background

Conventional cine phase-contrast MRI (Conv-PC) is the gold standard for blood flow measurements but can only provide flow measurements for an averaged heartbeat cycle (using cardiac gating). In contrast to Conv-PC, phase-contrast echo-planar MRI (EPI-PC) can be used to quantify the blood flow rate in real-time – giving the technique great potential for clinical and research applications. The objectives of the present *in vitro* study were to compare the accuracy of EPI-PC and Conv-PC and to assess the influence of pixel size and velocity encoding on flow measurements obtained with the two sequences.

Methods

Flow quantification was assessed using a pulsatile flow phantom. The flow rate curves were extracted with in-house post-processing software, and the flow curves from EPI-PC were reconstructed to give an average pulse cycle with 32 sampling points with the same waveform as that obtained with Conv-PC. Firstly, the accuracy of the EPI-PC was checked by comparing it with the flow rate in the calibrated phantom and the pulsation index from Conv-PC. Secondly, flow data from the two sequences were compared quantitatively as a function of the pixel size and the velocity encoding.

Results

The mean percentage difference between the EPI-PC flow rate and calibrated phantom flow rate was -2.9 %, which was within the confidence interval. The pulsatility indices for EPI-PC and Conv-PC were respectively 0.64 and 0.59. In order to keep the flow rate measurement error within 10%, the ROI in Conv-PC had to contain at least 13 pixels, while the ROI in EPI-PC had to contain at least 9 pixels. Furthermore, Conv-PC had a higher velocity-to-noise ratio and could use a higher velocity encoding than EPI-PC (20cm/s and 15cm/s, respectively).

Conclusions

The result of an *in vitro* study confirmed the accuracy of EPI-PC. Furthermore, EPI-PC was found to be less sensitive than Conv-PC at a low spatial resolution but was more sensitive than Conv-PC to velocity encoding.

Keywords: phase-contrast; echo-planar imaging; cine MRI; pulsatile flow; imaging phantom

Background

Conventional phase-contrast magnetic resonance imaging (Conv-PC) is a non-invasive technique that can be used to measure blood and cerebrospinal fluid (CSF) velocities. Conv-PC was used by Moran in 1982 to study flow velocities in humans [26]. In 1984, Bryant et al. used Conv-PC to produce flow velocity map [7]. The synchronization of cardiac movements with velocity measurements has been applied to MR velocity imaging [14,34]. Since then, Conv-PC has become a very important technique for *in vitro* studies and *in vivo* quantifications of blood and CSF flows [27,16,1,2,25,20,37].

Unfortunately, Conv-PC is limited by its relatively poor time resolution; it can only provide flow measurements for an averaged heartbeat cycle, which is reconstructed from all the acquired heartbeat cycles and uses gating. It is now known that breathing can affect CSF and cerebral blood flows [31,33]. Consequently, the flow velocities measured with Conv-PC may be breathing-dependent. Furthermore, Conv-PC is not able to reveal the effects of breathing on the dynamics of blood or CSF flows.

To overcome this limitation, several research groups have developed a fast acquisition method based on echo-planar imaging (EPI) in which a complete k-space can be acquired using one or a small number of pulse excitations [24,11]. In order to speed up data acquisition, Chen et al. combined EPI with a phase-contrast technique and thus introduced a novel sequence now commonly referred to as EPI-PC. This technique can be used to map CSF movements and demonstrate that CSF dynamics are influenced by breathing as well as by the cardiac cycle [8].

With a high time resolution (a sampling frequency of ~10 Hz), a shorter acquisition time, and a simpler acquisition process (i.e. no need for synchronization), EPI-PC has clear advantages in the field of research but also opens new opportunities for clinical practice. Recently, some researchers have used EPI-PC to quantify the influence of cardiac and respiratory pulses on the CSF and cerebral blood flow rates in the cranial system [39]. However, EPI-PC is more sensitive to eddy currents and has a longer readout window, resulting in a lower signal-to-noise ratio (SNR) than for Conv-PC [22,38]. Moreover, EPI-PC data is impacted by high-frequency, high-intensity gradient switching and by differences in magnetic susceptibility between blood and bone/air [35]. To the best of our knowledge, there are no published data on the accuracy of EPI-PC vs. Conv-PC.

The objectives of the present study were to quantitatively evaluate the accuracy of EPI-PC vs. Conv-PC and to assess the influence of pixel size and velocity encoding (VENC) on flow rate measurements. The acquisition parameters had to be optimized before EPI-PC could be validly compared with Conv-PC.

Material and Methods

Flow phantom

The phantom consisted of a series of four rigid, straight tubes (Tygon tubing, Saint-Gobain Performance Plastics, Akron, OH) with inner diameters of 9.5 mm (tube #1), 6.4 mm (tube #2), 4.4 mm (tube #3) and 2 mm (tube #4). The fluid flow was generated using a pulsatile flow pump. Six meters of tubing carried the fluid from the pump (located in the scanner control room) to the phantom's inlet. The phantom's outlet was connected to the tank that supplied water to the pump (Fig. 1 a).

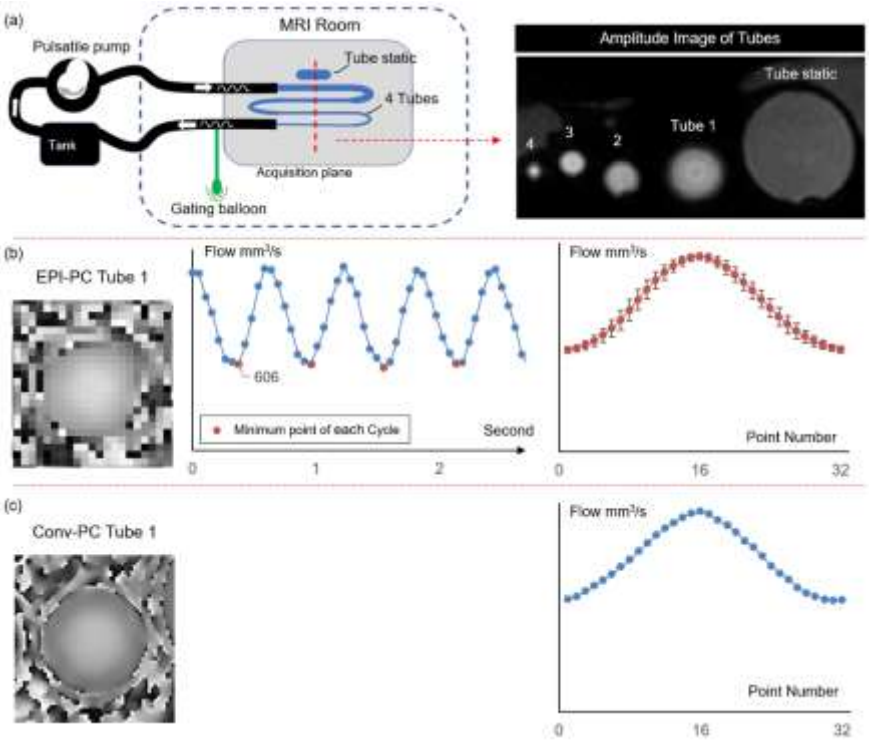

Figure 1 The flow phantom and the flow curve for the two sequences. **a** A realistic pulse-based model of the craniospinal system (left). An amplitude image for four tubes and a static tube in the acquisition plane (right), **b** An EPI-PC phase image (left) and its calibrated flow curve (middle) with the minimum (trough) points (in red) in each cycle found automatically by the software, which are used to separate the cycles. All the EPI-PC pulse cycles were used to reconstruct an average pulse cycle (right), **c** The Conv-PC phase image (left) and its calibrated flow curve.

To validate our system's flow rates, the pump was calibrated to deliver a clinically relevant flow rate (pulsatile flow with 99 bpm), and the volume collected from the phantom's output was recorded as a function of time. The true (calibrated) phantom flow rate was obtained through repeated measurements and was used as the reference value for calculation of the EPI-PC's accuracy. The present work covered measurements obtained with the first tube (diameter: 9.5 mm) only.

The flow phantom was positioned in the center of a head coil. On the return tube, a gating-compliant balloon was used to capture the frequency of the oscillation and thus to synchronize the acquisition of the Conv-PC with the flow rate waveform. A water-filled tube was positioned around the tubes, to define the static reference region.

Imaging procedure and method of comparison

All images were acquired on a 3T clinical scanner (Philips Achieva; maximum gradient: 80 mT/m; rate of gradient increase: 120 mT m^{-1} ms^{-1}). A 32-channel head coil was used to detect signals.

The EPI-PC sequence used in this experiment was a modified version of a standard, multi-shot, gradient-echo EPI sequence [30] with a Cartesian trajectory [4,9]. Typically, the velocity is encoded along the flow direction by positioning a bipolar gradient (with opposite polarity) behind the slice selection gradient. The spins of flowing tissue are at different locations relative to the bipolar gradient's positive and negative lobes. These spins are then confronted with the magnetic field gradients and accumulate a residual phase difference, whereas the stationary tissue does not experience a variation in the magnetic gradient. Phase data sets from before and after gradient reversal are subtracted to determine the "phase difference" of flowing spins, which is directly proportional to their underlying velocities. A description of the relationship between the measured phase and the velocities can be found in [28].

One of the objectives of the present study was to ensure that the optimized EPI-PC protocol could be applied in the clinic. Based on our clinical experience of Conv-PC, the imaging parameters are set to the initial values (field of view (FOV), VENC, etc.), except that the pixel size, flip angle and slice thickness (i.e., variable parameters) were set to different values within a small range; this improved the speed of imaging while maintaining image quality (Table 1).

	Initial parameters	**Tested parameters**	
		Conv-PC	EPI-PC
Pixel size (mm^2)	1×1	0.8×0.8 1.0×1.0 1.2×1.2	0.8×0.8 1.0×1.0 1.2×1.2

Thickness (mm)	3	2/3/4	2/3/4
Flip angle (degrees)	30	30	10/20/30
EPI factor	7	NA	3/5/7/9
FOV (mm^2)	100×60	100×60	100×60
VENC (cm/s)	5	5	5

Table 1 Initial and tested parameters for Conv-PC and EPI-PC. Abbreviations: Conv-PC, conventional cine phase-contrast MRI; EPI-PC, phase-contrast echo-planar imaging; EPI, echo-planar imaging; FOV, field of view; VENC, velocity encoding.

For each set of parameters, the EPI-PC and Conv-PC sequences were compared in terms of the segmentation error (expressed as a percentage of the difference between the segmented area and theoretical area), flow error (expressed as a percentage of the difference between the phantom flow rate and the measured flow rate), velocity-noise ratio (VNR), acquisition time, and sampling interval. This step was based on literature procedures for measuring the accuracy of phase contrast sequences [17,35]. We considered that the acceptable confidence intervals (CIs) for the segmentation error and the flow error were ±10%.

To compare the two sequences, a set of default parameters was obtained by selecting those for which (i) the segmentation error and flow error were within the CI, and (ii) the acquisition was the shortest. Once the default parameters had been selected, we evaluated the accuracy of the EPI-PC flow rate curve and also assessed the effects of pixel size and VENC on flow rate measurements for both sequences. To this end, the pixel size ranged from 0.8 mm to 3.2 mm in increments of 0.4 mm, whereas the VENC ranged from 5 cm/s to 25 cm/s in increments of 5 cm/s.

Statistical analysis

The reconstructed flow rate curves for the EPI-PC data and the Conv-PC data were compared in a Bland & Altman plot [5]. The influence of pixel size on flow rate was evaluated using a regression analysis. Pearson's test was used to analyze the correlation between variables. All statistical analyses were performed with R software (version 3.2.3, R Foundation for Statistical Computing, Vienna, Austria, www.r-project.org). The threshold for significance was set to $p<0.05$.

Software and postprocessing

To extract the flow rate curves, the MRI data were processed with in-house software (Flow [3,12]). Each Conv-PC series contained 32 phase images that were acquired to obtain a representative flow rate cycle (duration: 606 ms). Even though the acquisition time ranged from 13 to 33 s (depending on the spatial resolution), the interval between

two images (Δt) during an average cycle was constant (Δt = 19 ms). For EPI-PC series, the total number of acquired phase images was constant (n=150). The acquisition time ranged from 7 to 17 s, leading to a Δt that ranged from 46.7 ms to 113 ms. Six to 13 phase images were then reconstructed per cycle.

To minimize the effects of eddy current on the measurements, the velocity was calibrated by measuring the mean velocity in the static tube. Furthermore, to compare the two sequences, the EPI-PC flow rate signal was reconstructed over an average pulse cycle of 32 points with the same model as Conv-PC (Fig.1b); the reconstruction method is described below.

Regions of interest

By using the software's segmentation function, a region of interest (ROI) within the tube (ROI-Tube) can be automatically segmented on the phase image. The value of the segmented area can then be recorded. Likewise, a ROI withing the static tube (ROI-Reference) was manually defined as the source of velocity noise (Fig.2a, green cycle). For each phase image, the mean (V_{Ref}) and standard deviation (SD) (σ_{Ref}) velocity within ROI-Reference were calculated. The V_{Ref} and σ_{Ref} values were used to define a reference signal and an uneven signal, respectively (Fig.2b).

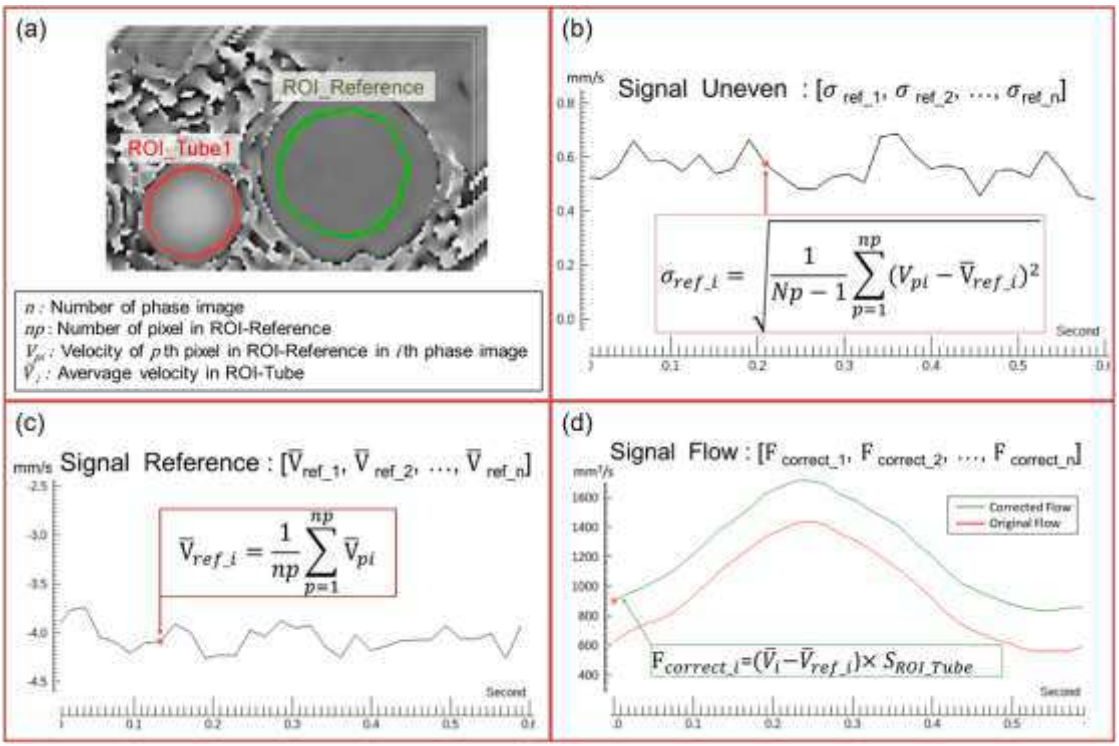

Figure 2 An example of Conv-PC postprocessing. **a** A representative segmented image obtained with software, with ROI-Tube#1 on tube #1 (in red) and ROI-Reference on the static tube (in green), **b** The uneven signal obtained from the SD of the velocity within the ROI-Reference in each phase image, **c** The reference signal constituted by the mean velocity within the ROI-Reference in each phase image, **d** The original flow curve (in red) for a pulse cycle extracted from the ROI-Tube, and the corrected flow curve (in green) calculated from the original flow and reference signals.

Calibration of the measured velocities

The calibration compensated for the noise error in the measurement of velocity. In theory, the measured velocity does not represent the true velocity, and the velocity in the ROI-Reference is null. To calculate the corrected (true) velocity, the measured velocity was subtracted from the V_{Ref} (Fig.2d).

Calculation of the VNR

The mean uneven signal $\overline{\sigma_{Ref}}$ was used to calculate the VNR by dividing the mean velocity in the ROI-Tube by the mean uneven signal in ROI-Ref (equation 1).

$$VNR = \frac{\bar{V}}{\overline{\sigma_{Ref}}} \quad \ldots\ldots (1)$$

Reconstruction of the mean EPI-PC cycle

The steps in the segmentation and calibration of the EPI-PC data were the same as for the Conv-PC data. After the flow rate signal has been obtained from the EPI-PC data, the software's cropping tool can be used to extract all the single pulse cycles from the original signal (red points in Fig.1b). A spline interpolation algorithm was then used to increase the number of sampling points to 32 for each pulse cycle in the EPI-PC data. The sampling points at each position and each pulse cycles were then averaged to obtain the corresponding flow rate value for the reconstructed average pulse cycle.

The pulsatility index

The pulsatility index was defined as follows [32]:

$$Pulsatility\ index = \frac{Max\ flow - Min\ flow}{Mean\ flow}$$

Results

Default parameters

After several repeated measurements, the phantom flow rate was found to be 1150 mm^3/s. The Reynolds number for the four tubes (calculated with the maximum velocity) ranged from 399 to 1260 and so was less than 2100; the flow was considered to be laminar. Table 2 shows how the main sequence parameters influenced the quality of the acquisition in Conv-PC and EPI-PC. As the pixel size increased, the Conv-PC acquisition time shortened but the

segmentation area and flow rate were still accurate. For EPI-PC, an increase in the pixel size from 0.8 mm to 1.2 mm was associated with 58% relative increase in the VNR and a 38% relative decrease in the acquisition time. Moreover, a slice thickness of 4 mm gave a higher VNR for both sequences.

Parameters for Conv-PC				**Results for Conv-PC**				
Pixel size (mm^2)	Thickness (mm^2)	Flip angle (degree)		Segmentation error (%)	Flow error (%)	VNR	Acquisition time (s)	Δt (ms)
0.8×0.8	3	30		2.3	2.3	16.2	33.8	18.9
1.0×1.0	3	30		6.8	1.7	19.9	26.3	18.9
1.2×1.2	3	30		8.3	4.5	15.9	23.2	18.9
0.8×0.8	**2**	30		13.3	5.8	10.9	33.8	18.9
0.8×0.8	**3**	30		2.3	2.3	16.2	33.8	18.9
0.8×0.8	**4**	30		3.1	6.0	17.9	33.8	18.9
Parameters for EPI-PC				**Results for EPI-PC**				
Pixel size (mm^2)	Thickness (mm^2)	Flip angle (degree)	EPI factor	Segmentation error (%)	Flow error (%)	VNR	Acquisition time (s)	Δt (ms)
0.8×0.8	3	30	7	6.9	7.0	4.6	20.1	134
1.0×1.0	3	30	7	4.4	0.9	5.8	13.5	90
1.2×1.2	3	30	7	3.4	7.4	7.3	12.5	83
1.0×1.0	**2**	30	7	6.1	1.0	3.8	14	93
1.0×1.0	**3**	30	7	4.4	0.9	5.8	13.5	90
1.0×1.0	**4**	30	7	0.0	3.4	7.4	13.4	89
1.0×1.0	3	**10**	7	2.5	1.7	2.6	13.5	90
1.0×1.0	3	**20**	7	1.7	2.6	4.5	13.5	90
1.0×1.0	3	**30**	7	4.4	0.9	5.8	13.5	90
1.0×1.0	3	10	**3**	4.4	4.3	2.4	26.9	179
1.0×1.0	3	10	**5**	5.2	2.4	2.9	15.5	103
1.0×1.0	3	10	**7**	2.5	1.7	2.6	13.5	90
1.0×1.0	3	10	**9**	0.8	6.7	3.0	10.2	68

Table 2. Results for Conv-PC and EPI-PC, as a function of different parameter values. Abbreviations: Conv-PC, conventional cine phase-contrast MRI; EPI-PC, phase-contrast echo-planar imaging; VNR, velocity-noise-ratio.

As expected, the flip angle had no effect on the imaging time but did influence the VNR. An increase in the flip angle from 10° to 30° was associated with a 123% relative increase in the VNR. Increasing the EPI factor decreased the acquisition time: changing the EPI factor from 7 to 9 reduced the acquisition time by 25% but barely impacted the segmentation area and flow rate measurements.

On the basis of these results, we selected the default parameters for comparing the two sequences (Table 3).

	Conv-PC	EPI-PC
FOV (F×P)	100×60	100×60
VENC (cm/s)	5	5
Pixel size (mm^2)	1.2×1.2	1.2×1.2
Thickness (mm)	4	4
Flip angle (degree)	30	30
EPI factor	NA	9
SENSE	1.5	2.5
TR (ms)	11	15.2
TE (ms)	7.7	9.1

Acquisition time (s)	23.6	9.3
Number of images per cycle	32	9.7

Table 3 The selected default parameters for Conv-PC and EPI-PC. Abbreviations: Conv-PC, conventional cine phase-contrast MRI; EPI-PC, phase-contrast echo-planar imaging; FOV, field of view; VENC, velocity encoding; EPI, echo planar imaging; SENSE, sensitivity encoding; TE, echo time; TR, repetition time.

Comparison of EPI-PC and Conv-PC sequences

The EPI-PC and Conv-PC sequences were applied to tube #1 with the selected default parameters.

After 10 measurements, the reconstructed EPI-PC and Conv-PC data were postprocessed to reconstruct the two average flow rate curves (Fig.3). The two curves were superimposed so that the peaks of the flow rates coincided on the time axis. The mean flow rates for EPI-PC and Conv-PC were 1116±25 mm^3/s and 1239±26 mm^3/s respectively, and the associated coefficient of variation was 2.3% in both cases. The pulsatility indices for EPI-PC and Conv-PC were respectively 0.64 and 0.59.

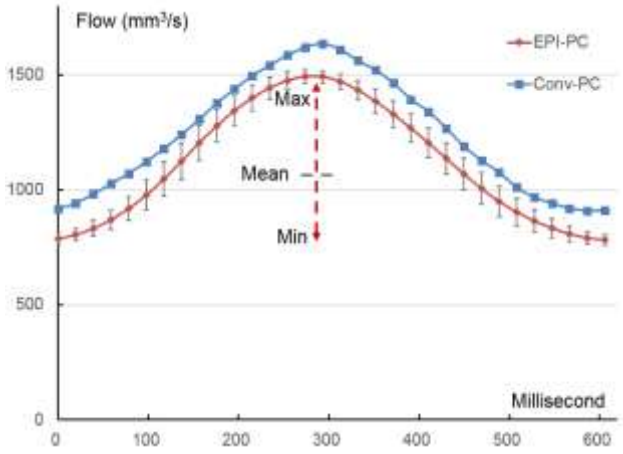

Figure 3 The average flow curves for Conv-PC (in blue) and EPI-PC (in red). The error bar on the EPI-PC reconstruction flow curve corresponds to the SD of each point.

A Bland–Altman plot (Fig.4) highlighted the differences between the EPI-PC and Conv-PC curves, with their 95% limits of agreement (dotted line). The differences between EPI-PC and Conv-PC data were plotted against the mean of the two measurements. The red line in the Figure shows the mean difference (-124 mm^3/s) for the 32 points. The two dotted lines on both sides of the red line indicate the 95% limits of agreement (-68 mm^3/s and -180 mm^3/s), calculated as the mean flow rate difference ± 1.96 × SD of the differences. All the points fell within the limits of agreement.

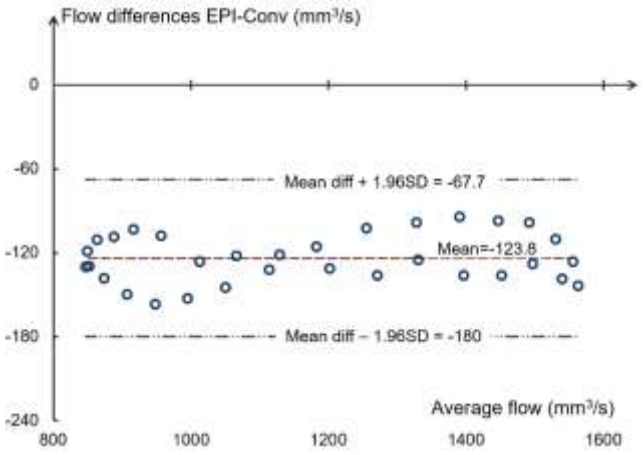

Figure 4 A Bland–Altman plot of the EPI-PC reconstruction flow curve and the Conv-PC flow curve for tube #1.

The influence of pixel size

In Fig. 5, the segmentation area (blue points) and the flow rate (red points) are shown as a function of pixel size. Each variable was measured four times. The blue shading corresponds to the CI for the theoretical segmentation area (70.8 mm^2 ± 10%) and the red shading corresponds to the CI for the flow rate (1150 mm^3/s ± 10%). For both sequences, the segmentation area and flow rate were positively correlated with the pixel size. The coefficient (R^2) for the correlation between flow rate and pixel size was 0.79 (*P<0.01*) for EPI-PC and 0.9 (*P<0.01*) for Conv-PC. The flow rates measurements obtained with EPI-PC were within the CI for pixel sizes of 1.2 mm to 2.8 mm. For Conv-PC, only pixel sizes of 1.2 mm to 2.4 mm provided flow rates within the CI.

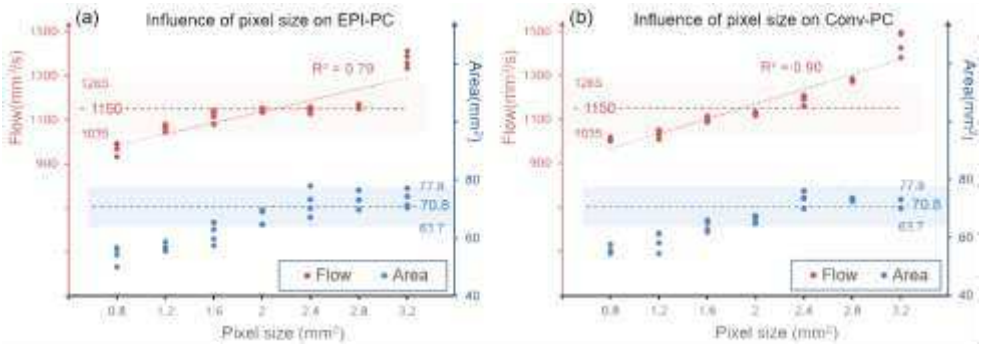

Figure 5 Segmentation area (on the right y-axis, in blue) and flow rates (on the left y-axis, in red) for two sequences with different pixel sizes (on the X-axis). **a** EPI-PC, **b** Conv-PC

The distributions of the segmentation area (on the x axis) and flow rate (on the y axis) of the two sequences are shown in Fig.6. The purple and green shadings correspond to the CI of the segmentation area and the flow rate, respectively.

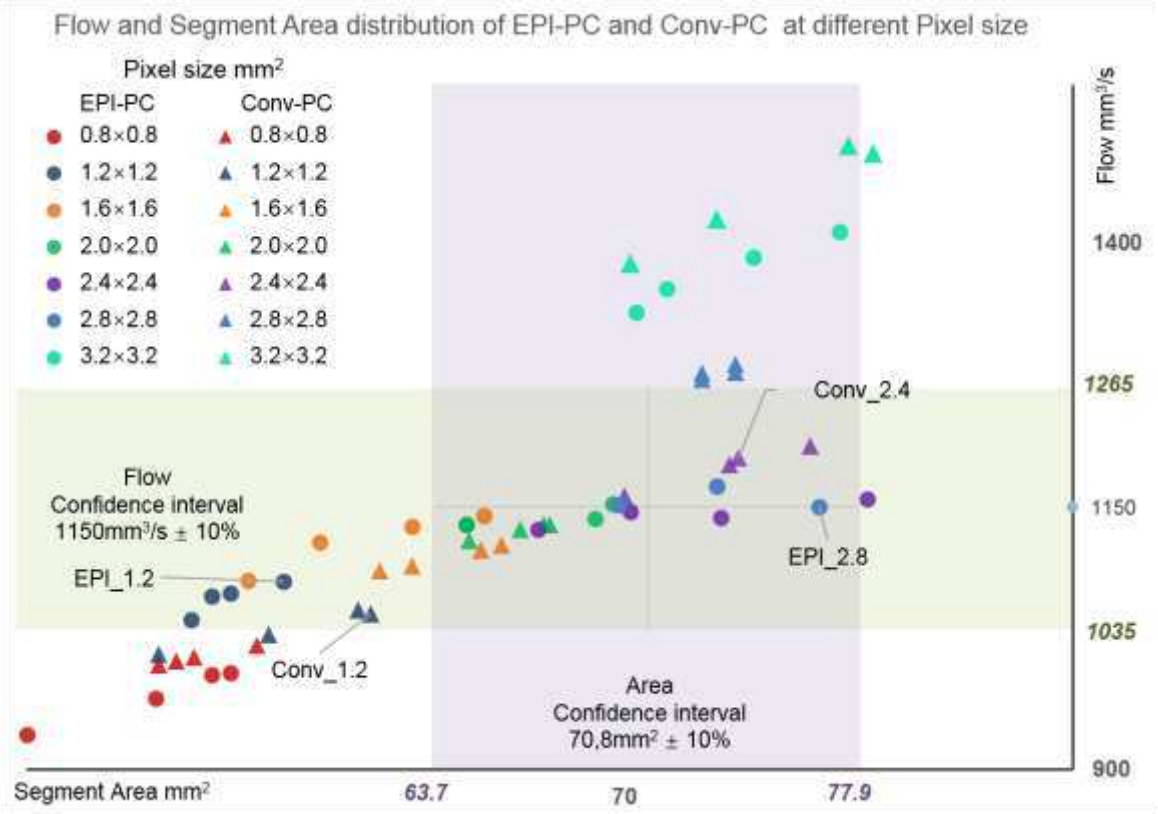

Figure 6 Distribution of the segmentation area & flow rate for EPI-PC and Conv-PC, as a function of the pixel size (depicted by different color levels).

Fig.7 shows the VNR of EPI-PC and Conv-PC with different pixel sizes. For a pixel size of 1.2 mm to 2.8 mm, the VNR increased for EPI-PC but did not change for Conv-PC. For each pixel size, the VNR was higher for Conv-PC than for EPI-PC.

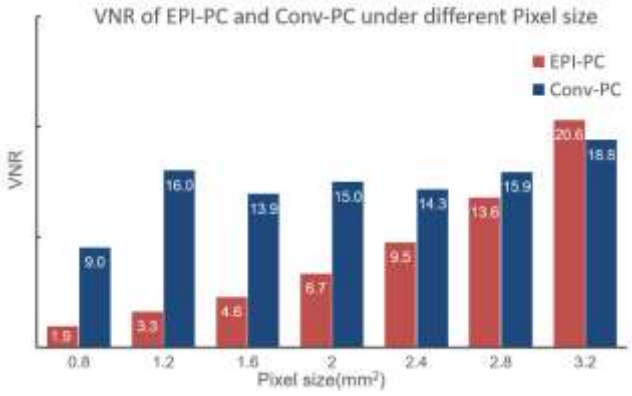

Figure 7 The VNR for EPI-PC and Conv-PC sequences, as a function of the pixel size.

The influence of VENC

Fig.8 shows the influence of VENC on EPI-PC and on Conv-PC. As the VENC increased, the accuracy decreased more rapidly for EPI-PC than for Conv-PC. With a VENC of 15 cm/s, the segmentation area for EPI-PC was outside

the CI. Moreover, with a VENC of 20 cm/s, the flow rate for EPI-PC was also outside of the CI. For a VENC of 25 cm/s or more, the software was not able to segment the ROI. In contrast, with a VENC below 20 cm/s, the flow rates for Conv-PC were within the CI.

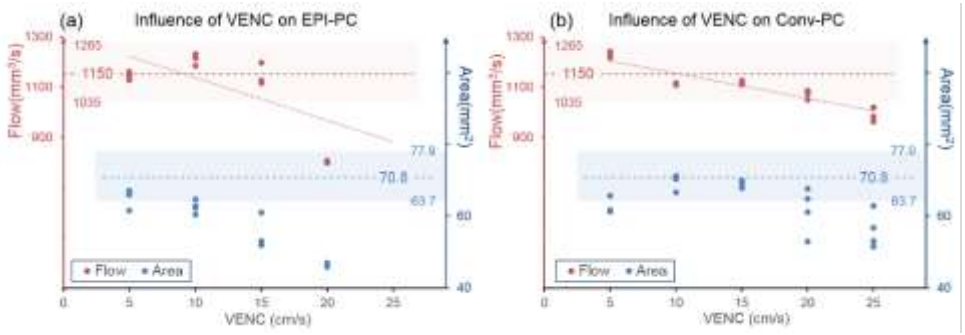

Figure 8 Segmentation area (on the right y-axis, in blue) and flow rates (on the left y-axis, in red) for two sequences with five different VENC values (on the X-axis). **a** EPI-PC, **b** Conv-PC.

Fig.9 gives the VNR for EPI-PC and Conv-PC with different VENC values. As the value of VENC increased, the VNR for EPI-PC fell from 3.6 to 0.8. For Conv-PC, the VNR fell from 27.2 to 8.1 as the VENC value increase from 5 cm/s to 15 cm/s. For VENC values of 15 cm/s to 25 cm/s, the VNR varied less (mean ± SD = 8.4 ± 0.76). Overall, the VNR with different VENC values was much greater for Conv-PC than for EPI-PC.

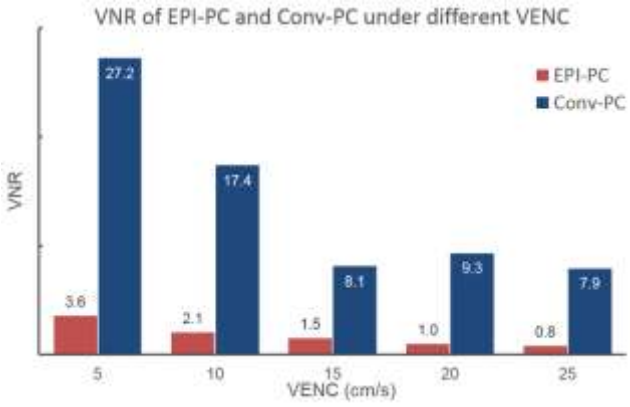

Figure 9 The VNR for EPI-PC and Conv-PC sequences, as a function of the VENC.

Discussion

In the present study, a pulse-based phantom model was used to generate a constant pulse wave with velocities similar to those of CSF and venous blood flows. Our objective was not only to check the accuracy of the mean flow rate measured with EPI-PC but also to compare the shape of the flow rate curve with that determined by Conv-PC, which

had a smaller sampling interval (i.e. the gold standard). In order to compare EPI-PC and Conv-PC, the real-time flow rate signal for the EPI-PC curve was reconstructed to give the same 32-point flow rate curve as for Conv-PC.

Definition of default parameters

The Conv-PC sequence was able to complete several phase encodings during each pulse cycle and to fill them into the different phase images' K-space; even though the acquisition time increased, it did not therefore affect the pseudo-sampling interval Δt. However, for the real-time imaging with EPI-PC, the acquisition time was directly related to Δt; hence, increasing the sampling frequency could improve the accuracy of the reconstructed curve. The protocol's default parameters were chosen to achieve a higher sampling frequency while maintaining the accuracy of the segmentation area and flow rate measurements.

The effects of magnetic field inhomogeneity must also be taken account, since the reference tube was not positioned around the flow tube in the FOV [19,10]. Therefore, the estimated VNR in this work was a pseudo-VNR averaged across all images. This measurement method is likely to be more conveniently and might be sufficient for comparing the VNRs from several different sequences.

In single-shot EPI, all the lines in K-space are filled by switching the frequency-encoding gradient after a single excitation pulse. In contrast, for multi-shot EPI, the k-space is segmented into multiple shots, which are filled through multiple TR periods. The number of lines per segment is called the "EPI factor " or the "echo train length" and has a great influence on the sampling frequency. The single-shot EPI has a higher sampling frequency and a lower VNR, and so is more likely to be sensitive to geometric distortion [13]. The multi-shot EPI is less sensitive to geometric distortions, given the shorter readout time [21]. This is why we used a multi-shot EPI in the present study.

When the EPI factor is fixed and the number of phase-encoding lines is reduced, the sampling frequency can still be increased. With sensitivity encoding (SENSE), the reduction in phase-encoding lines depends on the number of coils used for parallel data acquisition [29]. In our experiment, the SENSE value was 2.5 for EPI-PC and 1.5 for Conv-PC.

Comparison of EPI-PC and Conv-PC

Using the default parameters, the respective flow rate measurements for the two sequences were both within the CIs and did not exceed 8% [15] (flow rate error: -2.9% for EPI-PC vs. 7.8% for Conv-PC).

With the default protocol, each EPI-PC cycle contained 10 sampling points. By comparing the reconstructed flow rate curves for EPI-PC and Conv-PC and considering a waveform similar to that observed for venous blood and CSF, the difference in the pulsatility index between EPI-PC and Conv-PC was less than 10%. The errors for the corresponding 32 points in the two curves were all within the limits of agreement (Fig. 4). Furthermore, the Conv-PC technique could use multiple pulse cycles to gradually fill a K-space for 32 phase images; hence, the flow rate curve for Conv-PC was described by only 32 characteristic points. For EPI-PC with the default parameters, only 9 or 10 characteristic points were used to describe a pulse cycle, and the reconstructed flow rate curve was smoother than that for Conv-PC. Therefore, EPI-PC is more suitable for flows with gentle fluctuations, such as venous blood and CSF. However, EPI-PC has limitations for reconstructing high-frequency fluctuations, such as certain arterial waveforms. Increasing the EPI-PC sampling frequency is likely to improve the accuracy of the corresponding reconstructed curve.

The influence of pixel size

The EPI-PC sequence was less sensitive to pixel size than Conv-PC. Due to the characteristics of laminar flow, the velocity is lower at the boundary of the tube than in its center. When the resolution is high, the flow at the tube wall did not produce a large phase difference. Hence, this area can be considered to be non-flowing on the phase contrast image, and so the true segmented area is smaller than the theoretical area (Fig.6).

Accurate segmentation area and flow rate measurements were possible with a range of pixel sizes: from 1.8 to 2.8 mm for EPI-PC and from 1.8 to 2.4 mm for Conv-PC. Within these ranges, the measured flow rate was slightly influenced by the segmentation area. As the pixel size continued to increase (above 2.8 mm for EPI and above 2.4 mm for Conv-PC), the flow rate of the two sequences began to exceed the boundaries of the CI (Fig.6). We hypothesize that a partial volume effect led to overestimation of the velocity [35,6]. As a result, the flow rate error was too large - even though the segmentation region was within the CI.

Therefore, in order to measure the flow rate accurately, the pixel size for Conv-PC should be less than 25% of the target ROI diameter; in other words, the ROI should comprise at least 13 pixels. Our result is in line with those obtained by Greil et al. and Tang et al., who confirmed that a minimum of 16 pixels within the Conv-PC ROI was required to keep the flow rate error within 10% [17,35]. For the EPI-PC sequence, the pixel size should be less than 30% of the diameter of the target vessel/CSF; in other words, the ROI should have at least 9 pixels.

The influence of VENC

The EPI-PC sequence was more sensitive to variations in VENC. Without aliasing, the VNR is inversely proportional to the VENC [23,28,18]. This sensitivity was also reflected in our experiments by the pseudo-VNR (Fig.10). Using different VENC values, the VNR was much greater for Conv-PC than for EPI-PC. Firstly, this was because the Conv-PC can use multiple cycles to fill a phase image, and so the influence of noise on the echo signal is smaller. For EPI-PC, multiple phase encodings are needed to complete the K-space during a TR, so the SNR of the echo signal is much smaller and the VNR of the phase image is relatively low. Secondly, and in order to increase the sampling frequency in the EPI-PC sequence, the SENSE value in our experiment was set to 2.5; this was 66% greater than the value for Conv-PC (1.5).

Since the VNR was higher for Conv-PC than for EPI-PC, the increase in VENC had relatively little influence on the accuracy of Conv-PC flow rate measurements. Even when the VENC increased from 5 cm/s to 20 cm/s, the flow rate measured with Conv-PC was still within the CI. In contrast, the maximum value for VENC in the EPI-PC sequence was 10 cm/s; above this value, the segmentation was inaccurate.

The decrease in VNR mainly affects the segmentation of phase images; segmentation errors can arise when the pixel intensity in the phase image of the target vessel is close to that of the surrounding (non-flowing) tissue. This effect can be reduced if the magnitude image is segmented.

Limitations and perspectives

Firstly, the phantom waveform in our study was sinusoidal, whereas there are two higher-frequency harmonics (2-4 Hz) in the cerebral arterial waveform. Hence, the ability of EPI-CP to accurately quantify the arterial waveform will now have to be demonstrated in *in vivo* studies. Secondly, the phantom model did not take account of arrhythmic and respiratory effects, for which the EPI-PC sequence is advantageous because (in contrast to Conv-PC) it does not require synchronization with the cardiac cycle.

Conclusion

We used a segmentation algorithm and flow rate curve reconstruction to determine the accuracy of EPI-PC. When using the selected default parameters, the calculated error between the reconstructed EPI-PC curve and the Conv-PC curve was small. Increasing the sampling frequency gave a more detailed view of the EPI-PC sequence's curve.

Compared with Conv-PC, EPI-PC can be adapted to increase the spatial resolution but is more sensitive to VENC. An excessively small pixel size reduced the VNR and the sampling frequency, while an excessively large pixel size produced partial-volume effects and an overestimation of the flow rates.

Our study shows that setting the pixel size of the EPI-PC to 33% of the diameter of the water tube gives the best VNR and temporal resolution without causing partial volume effects, and to obtain a higher VNR, VENC should be set small (aliasing needs to be avoided). These results provided reference values for the clinical application of EPI-PC.

List of abbreviations

Conv-PC: conventional cine phase-contrast MRI

CI: confidence interval

CSF: cerebrospinal fluid

EPI: echo-planar imaging

EPI-PC: phase-contrast echo-planar MRI

FOV: field of view

ROI: region of interest

ROI-Reference: ROI withing the static tube

V_{Ref}: mean velocity within ROI-Reference

σ_{Ref} : standard deviation velocity within ROI-Reference

VENC: velocity encoding

VNR: velocity-noise ratio

SD: standard deviation

SENSE: sensitivity encoding

SNR: signal-to-noise ratio

Δt : time interval between two images

Declarations

Ethics approval and consent to participate

Not applicable

Consent for publication

Not applicable

Availability of data and materials

The datasets used and/or analysed during the current study are available from the corresponding author on reasonable request.

Competing interests

The authors declare that they have no conflicts of interest with respect to the research, authorship, and/or publication of this article. The figures are original and have not been published previously.

Funding

This research was funded by the GIE Facing Faces and the French National Research Agency (Hanuman project; reference: ANR-18-CE45-0014).

Authors' contributions

LP designed the study, developed the post-processing software, and wrote the initial draft of the manuscript. SF performed statistical analysis of the data and revised the manuscript. MA collected and analyzed the in vitro data. Ob developed the post-processing software and revised the manuscript. All authors approved the final version of the manuscript for submission. All authors read and approved the final manuscript.

Acknowledgements

The authors thank David Chechin for scientific support and the staff members at the Facing Faces Institute (Amiens, France) for technical assistance.

Authors' information

Dr Pan Liu received his PhD in Radiological and Medical Physics from the Jules Verne University of Picardy (Amiens, France) in 2021. He is currently funded as a postdoctoral fellow through the CHIMERE-UR7516 research group. His main research interests are MRI image processing algorithms and image processing software development.

Dr Sidy Fall received a PhD in Biomedical Engineering from the Jules Verne University of Picardy (Amiens, France) in 2009. He is currently an engineer at the university's Preclinical MRI Facility. His main research interests are MRI and physiological data processing and especially functional MRI, DTI, and vascular imaging.

Maureen Ahiatsi received a Master's Degree in Neurosciences – Neurobiology from the University of Grenoble Alpes (Grenoble, France) in 2020. She is currently studying for a Master's Degree in Artificial Intelligence and Digital Transformation at the AI & Digital Transformation School (Paris, France). Her research interests include brain pathophysiology, and medical imaging data processing and analysis.

Dr Olivier Baledent received a PhD on the MRI-based imaging of CSF and blood flow using at the Jules Verne University of Picardy (Amiens, France) in 2001. He is currently an assistant professor at the university and also heads the Medical Image Processing Department at Amiens University Medical Center (Amiens, France), where he is developing flow MRI techniques in the CHIMERE-UR7516 research group. In 2020, he helped to create "neurofluid imaging" as a new section in the International Society of Magnetic Resonance Imaging.

References

1. Alperin NJ, Sang HL, Lots F, et al. MR-Intracranial Pressure (ICP): A Method to Measure Intracranial Elastance and Pressure Noninvasively by Means of MR Imaging: Baboon and Human Study. Radiology. 2000;217(3):877-885.
2. Balédent O, Gondry-Jouet C, Stoquart-Elsankariet S, et al. Value of Phase Contrast Magnetic Resonance Imaging for Investigation of Cerebral Hydrodynamics. J Neuroradiology. 2006;33(5):292-303
3. Balédent O, Henry-Feugeas MC, Idy-Peretti I. Cerebrospinal Fluid Dynamics and Relation with Blood Flow: A Magnetic Resonance Study with Semiautomated Cerebrospinal Fluid Segmentation. Invest Radiol, 2001;36(7): 368-377.
4. Benjamin, A. J. V., Gómez, P. A., Golbabaee, M., et al. Multi-shot Echo Planar Imaging for accelerated Cartesian MR Fingerprinting: an alternative to conventional spiral MR Fingerprinting. Magnetic resonance imaging. 2019; 61:20-32.
5. Bland JM, Altman DG. STATISTICAL METHODS FOR ASSESSING AGREEMENT BETWEEN TWO METHODS OF CLINICAL MEASUREMENT. Lancet. 1986;327(8476):307-310
6. Bouillot P, Delattre BMA, Brina O, et al. 3D Phase Contrast MRI: Partial Volume Correction for Robust Blood Flow Quantification in Small Intracranial Vessels. Magn Reson Med. 2018;79:129-140.
7. Bryant DJ, Payne JA, Firmin DN, Longmore DB. Measurement of Flow with NMR Imaging Using a Gradient Pulse and Phase Difference Technique. J Comput Assist Tomo. 1984;8(4):588-593.
8. Chen L, Vu AT, Xu S, et al. Evaluation of Highly Accelerated Simultaneous Multi-Slice EPI for FMRI. NeuroImage. 2015;104:452-459.
9. DeLaPaz, R. L. Echo-planar imaging. Radiographics. 1994;14(5):1045-1058.
10. Dyverfeldt P, Bissell M, Barker AJ, et al. 4D Flow Cardiovascular Magnetic Resonance Consensus Statement. J Cardiovasc Magn R. 2015;17(1):1-19.
11. Edelman RR, Wielopolski P, Schmitt F. Echo-planar MR imaging. Radiology. 1994;192(3): 600-612.
12. Fall S, Pan L, Balédent O. A Semi-Automatic Software for Processing Real-Time Phase-Contrast MRI Data. In: VipIMAGE 2019. 2019;34: p. 22-28.
13. Farzaneh F, Riederer SJ, Pelc NJ. Analysis of T2 Limitations and Off-Resonance Effects on Spatial Resolution and Artifacts in Echo-Planar Imaging. Magn Reson Med. 1990;14(1):123-139.
14. Feinberg DA, Mark AS. Human Brain Motion and Cerebrospinal Fluid Circulation Demonstrated with MR Velocity Imaging. Radiology. 1987;63(3):793-799
15. Garg P, Westenberg JJM, et al. Comparison of Fast Acquisition Strategies in Whole-Heart Four-Dimensional Flow Cardiac MR: Two-Centre, 1.5 Tesla, Phantom and in Vivo Validation Study. J Magn Reson Imaging. 2018;47(1):272-281.
16. Greitz D, Franck A, Nordell B. On the Pulsatile Nature of Intracranial and Spinal CSF-Circulation Demonstrated by MR Imaging. Acta Radiol. 1993;34(4):321-328
17. Greil G, Geva T, Maier SE, Powell AJ. Effect of Acquisition Parameters on the Accuracy of Velocity Encoded Cine Magnetic Resonance Imaging Blood Flow Measurements. J Magn Reson Imaging. 2002;15:47-54.
18. Ha H, Kim GB, Kweon J, et al. Multi-VENC Acquisition of Four-Dimensional Phase-Contrast MRI to Improve Precision of Velocity Field Measurement. Magn Reson Med. 2016;75(5):1909-1919.
19. Ha H, Park KJ, Dyverfeldt P, et al. In Vitro Experiments on ICOSA6 4D Flow MRI Measurement for the Quantification of Velocity and Turbulence Parameters. Magn Reson Imaging. 2020;72:49-60.

20. Hoppe M, Heverhagen, JT, Froelich JJ, et al. Correlation of Flow Velocity Measurements by Magnetic Resonance Phase Contrast Imaging and Intravascular Doppler Ultrasound. Invest Radiol. 1998;33(8):427–432.
21. Holdsworth SJ, Skare S, Newbould RD, et al. Readout-Segmented EPI for Rapid High-Resolution Diffusion Imaging at 3T. Eur J Radiol. 2008;65(1):36-46.
22. Kim, Y. J., Kim, S. H., Kang, B. J., Park, C. S., Kim, H. S., Son, Y. H., & Song, B. J. Readout-segmented echo-planar imaging in diffusion-weighted mr imaging in breast cancer: comparison with single-shot echo-planar imaging in image quality. Korean J Radiol. 2014;15(4):403-410.
23. Lee AT, Pike GB, Pelc NJ. Three-point phase-contrast velocity measurements with increased velocity-to-noise ratio. Magn Reson Med. 1995;33:122–126.
24. Mansfield P. Multi-Planar Image Formation Using NMR Spin Echoes. J. Phys. C: Solid State Phys. 1977;10(3):55–58.
25. McCauley TR, Pena CS, Holland CK, et al. Validation of Volume Flow Measurements with Cine Phase-Contrast MR Imaging for Peripheral Arterial Waveforms. J Magn Reson Imaging. 1995;5:663-68.
26. Moran PR. A Flow Velocity Zeugmatographic Interlace for NMR Imaging in Humans. Magn Reson Imaging. 1982;1(4):197-203.
27. Nayler GL, Firmin DN, Longmore DB. Blood Flow Imaging by Cine Magnetic Resonance. J Comput Assist Tomo. 1986;10(5):715-722.
28. Pelc NJ, Herfkens RJ, Shimakawa A, Enzmann DR. Phase Contrast Cine Magnetic Resonance Imaging. Magn Reson Q. 1991;7(4): 229-54.
29. Pruessmann KP, Weiger M, Scheidegger MB, Boesiger P. SENSE: sensitivity encoding for fast MRI. Magn Reson Med. 1999;42:952–962.
30. Romero JM, Liberato AC, Montes D, et al. Accuracy of MRI T2*-weighted sequences (GRE-EPI) compared to CTA for detection of anterior circulation large vessel thrombus. Emergency radiology. 2020;1-7.
31. Schroth G, Klose U. Cerebrospinal Fluid Flow. II. Physiology of Respiration-Related Pulsations. Neuroradiology. 1992;35(1):10-15.
32. Schubert T, Pansini M, Bieri O, et al. Attenuation of blood flow pulsatility along the Atlas slope: a physiologic property of the distal vertebral artery? AM J NEURORADIOL. 2015;36(3):562-567.
33. Skytioti M, Sovik S, Elstad M. Respiration-Related Cerebral Blood Flow Variability Increases during Control-Mode Non-Invasive Ventilation in Normovolemia and Hypovolemia. Eur J Appl Physiol. 2017;117(11):2237-2249.
34. Spraggins TA. Wireless Retrospective Gating: Application to Cine Cardiac Imaging. Magn Reson Imaging. 1990;8(6):675-681.
35. Stanescu T, Wachowicz K., & Jaffray DA. Characterization of tissue magnetic susceptibility-induced distortions for MRIgRT. Medical Physics. 2012;39(12):7185-7193.
36. Tang C, Blatter DD, Parker D. Accuracy of Phase-Contrast Flow Measurements in the Presence of Partial-Volume Effects. J Magn Reson Imaging. 1993;3(2):377-385.
37. Wåhlin A, Ambarki K, Birgander R, et al. Measuring Pulsatile Flow in Cerebral Arteries Using 4D Phase-Contrast MR Imaging. Am J Neuroradiol. 2013;34(9):1740-45.
38. Wu W, & Miller KL. Image formation in diffusion MRI: a review of recent technical developments. J Magn Reson Imaging. 2017;46(3):646-662.
39. Yildiz S, Thyagaraj S, et al. Quantifying the Influence of Respiration and Cardiac Pulsations on Cerebrospinal Fluid Dynamics Using Real-Time Phase-Contrast MRI. J Magn Reson Imaging. 2017;46(2):431-439.

Supplementary Files

This is a list of supplementary files associated with this preprint. Click to download.

- GraphicalAbstractLIUPan.tif